J. Fluid Mech. (1971), *vol.* 50, *part* 2, *pp.* 233–255
Printed in Great Britain

Structural features of turbulent flow over smooth and rough boundaries

By A. J. GRASS

Department of Civil and Municipal Engineering,
University College, London

(Received 26 August 1970 and in revised form 28 June 1971)

An experimental study of boundary-layer turbulence in a free surface channel flow is described. Attention is concentrated on the effects of different surface roughness conditions on the turbulence structure in the boundary region. Hydrogen bubble flow tracers and medium high-speed motion photography were used to obtain an instantaneous visual and quantitative description of the flow field. In particular it proved possible to record instantaneous longitudinal and vertical velocity profiles from which distributions of the instantaneous Reynolds stress contribution were computed.

Two well-defined intermittent features of the flow structure were visually identified close to the boundary. These consisted of fluid ejection phases, previously reported by Kline *et al.* (1967) for smooth boundary flow, and fluid inrush phases. Conditional averaging of the instantaneous velocity data yielded quantitative confirmation that ejection phases corresponded with ejection of low momentum fluid outwards from the boundary whilst inrush phases were associated with the transport of high momentum fluid inwards towards the boundary. Inrush and ejection events were present irrespective of the surface roughness condition.

Conditional averaging also indicated that both inrush and ejection sequences correlate with an extremely high contribution to Reynolds stress and hence turbulence production close to the boundary. Indeed the present results, taken with those from previous studies, suggest that turbulence production is dominated by the joint contribution from the inrush and ejection events. It is emphasized that these structural features are intermittent, forming important linked elements of a randomly repeating cycle of wall-region turbulence production which is apparently driven by some violent three-dimensional instability mechanism.

Whilst the most coherent effects of the observed inrush phases appear to be mainly confined to a region close to the boundary, the influence of the ejection phases is far more extensive. The ejected low momentum fluid elements, drawn from the viscous sublayer and from between the interstices of the roughness elements, travel outwards from the boundary into the body of the flow and give rise to very large positive contributions to Reynolds stress at points remote from the boundary. This effect is sufficiently strong to prompt the suggestion that the ejection process could represent a universal and dominant mode of momentum

transport outside the immediate wall region and possibly extending across the entire thickness of the boundary layer.

A structural model based on the present observations is seen to exhibit consistency with many commonly visualized features and recorded average properties of turbulent boundary-layer flows in general.

1. Introduction

A primary objective of the experimental programme described in this paper was to obtain detailed measurements of turbulent velocity fluctuation characteristics close to boundaries of varying roughness in a two-dimensional water channel flow. This information was required in the broader context of a concurrent study of sediment transport mechanics. At the time when the tests were carried out very few reliable water turbulence measurements were available primarily because of a lack of suitable instrumentation. The method adopted for the measurements was the hydrogen bubble technique largely developed at Stanford University and described in detail by Schraub *et al.* (1964). Whilst tedious in quantitative analysis this technique has the major advantages of excellent flow visualization, multipoint instantaneous velocity sampling over a large flow region and quantitative accuracy and reliability. These powerful facilities proved invaluable not only in measuring the required boundary region turbulence characteristics but also in carrying out a quantitative study and interpretation of certain observed large-scale features of the turbulence structure responsible for the fluctuating field close to the bed. The latter observations form an important element of the work reported below.

The analytical intractability of the turbulent shear flow problem has inevitably tended to direct a large proportion of research effort along experimental lines. Experimental studies have in turn been frustrated by the inherent complexity of the turbulent flow structure which makes visual observation and quantitative measurement extremely difficult. It is perhaps not surprising therefore that, to date, a physically realistic model which adequately relates the large eddy structure and momentum transfer mechanisms of turbulent boundary layers to the mean velocity field is still lacking. Substantial progress has been made towards the evolution of such a model however, mainly through interpretation of velocity correlation measurements such as those due to Grant (1958), Favre, Gaviglio & Dumas (1957, 1958) and more recently by the visualization approaches of Kline *et al.* (1967), Kim, Kline & Reynolds (1968) and Corino & Brodkey (1969). The visualization studies have, for example, produced evidence partially supporting Townsend's (1957) and Grant's (1958) postulation that an eddy structure consistent with velocity correlation measurements could take the form of jets of low momentum fluid issuing from the boundary region. This corroboration is significant since, as Townsend pointed out, the inference of eddy structure from the double velocity correlation function is certainly not a unique procedure. In addition, the long-term averaging used in the early correlation measurements tends to obscure any intermittent features of the flow struc-

ture, which obstructs full understanding of the physical mechanisms involved. This latter disadvantage and the importance of short-term conditional averaging, as used for example by Kim *et al.*, have been discussed in some detail by Mollo-Christensen (1970).

Inference of flow structure from visualization studies also presents considerable difficulties. First, the perception of pattern in a randomly fluctuating velocity field requires a considerable degree of structural organization in the flow. It is fortunate that the structure of boundary-layer turbulence appears to possess such coherence immediately adjacent to smooth boundaries. Further away from a smooth boundary and in the case of rough boundary flow the problem of pattern recognition becomes increasingly difficult. This is well illustrated by the visualization photographs presented by Kline *et al.* (1967). Second, even if some general structural feature is discernable the selection of a conditional averaging procedure to abstract quantitative and reproducible information poses further problems. A good example of these difficulties was encountered by Kim *et al.* when faced with the task of deciding precisely what did and what did not constitute a viscous sublayer ejection sequence and also in defining the beginning and end of such sequences. Similar problems have arisen in investigating the constituent details of the flow structure associated with the intermittent region of boundary layers as discussed recently by Kovasznay, Kibens & Backwelder (1970). These difficulties were inevitably encountered in the portion of the present work concerned with boundary-layer flow structure.

The hydrogen bubble technique places specially organised tracers into the flow in a strict geometric pattern. In addition, the vertical orientation of the probe wire used in the present experiments released lines of bubble tracers virtually coincident with the instantaneous longitudinal (streamwise) velocity profiles occurring in the boundary layer. This tended to optimize the observers' chances of discerning any visually apparent eddy patterns in the flow structure. Close study of the high-speed film records did in fact reveal the following general structural features. The instantaneous longitudinal velocity profiles appeared to oscillate randomly about some average profile. Oscillations did not take the form of local spikes on the mean profiles but exhibited strong correlation over large portions of the visible flow depth. Ejection of low momentum fluid from the boundary region was visually quite clearly correlated with low longitudinal velocity phases as previously observed by Kline *et al.* and Corino & Brodkey. In addition, fluid inrush phases were also apparent where the instantaneous longitudinal velocity profiles passed through the mean, producing high longitudinal velocities close to the bed. These inrush sequences visually correlated with negative vertical velocities carrying fluid inwards towards the boundary (see figure 8(*a*)–(*c*), plates 2–4).

Intuitively, it seems reasonable to anticipate that these observed extreme deviations in longitudinal velocity profile shape, about the mean, might be the result of extreme manifestations of an underlying disturbance mechanism. This prompted the present choice of a simple conditional sampling procedure which concentrates attention on the flow structure during periods when the streamwise velocity shows maximum excursion from its local average value (see

§4.5 below). A major objective was to obtain quantitative confirmation of a disturbance mechanism and turbulence production process strongly associated with and possibly dominated by randomly intermittent inrush ejection cycles.

2. Experimental apparatus and measurement techniques

2.1. *Flow channel*

Three experiments, corresponding to hydraulically smooth, transitional and rough boundary conditions, were performed in an open topped glass sided channel 10 m long by 25 cm wide. Water was recirculated through the channel via a high-precision constant head tank. The rate of flow was controlled by means of an inlet spear valve and measured volumetrically using a dump tank at the outlet end of the channel. Water depths were adjusted by means of an overshoot weir and measured using a micrometer pointer gauge.

The depth of flow was kept constant for all three experiments at approximately 5 cm in the region of the test section located 6·5 m downstream from the channel inlet. This yielded a depth to width ratio of 1:5 designed to ensure reasonably two-dimensional flow and freedom from wall effects at the centre of the channel. The two-dimensionality of the flow was checked using a micro-propeller velocity meter which was traversed across the channel at a height of 2·5 cm above the bed. These measurements showed that the local mean streamwise velocity varied by less than 3% over the centre 12·5 cm of the channel width.

The overall average flow velocity was also kept constant at approximately 14·5 cm/sec by maintaining a constant flow rate for the tests. Flow Reynolds number, based on average velocity and flow depth, was thereby held constant at approximately 7000 in all three experiments.

The energy grade line down the channel resulted in a small difference in depth between channel inlet and outlet. In the most extreme case, with the rough boundary condition, this produced a maximum difference of 5% in velocity between the inlet and outlet ends of the channel. This slight divergence from strictly uniform flow conditions was considered sufficiently small to be ignored for the purposes of the present experiments.

Measurements with the micrometer depth gauge indicated maximum fluctuations in water surface elevation of order $\pm$ 0·2 mm. These disturbances resulted from high frequency surface waves generated by the flow turbulence and not from any longer-term cyclic variations in the recirculatory system.

Preliminary tests showed that the inlet boundary layer, which was tripped by means of a 2·5 mm diameter wire in the smooth boundary case, grew to intersect the free surface at approximately 2 m downstream from the channel inlet. The flow therefore reached the test section in a fully developed condition.

2.2. *Boundary roughness*

The hydraulically smooth, transitional and rough boundary conditions were achieved by covering the channel bed with polyurethane varnished marine plywood, 2 mm (7–10 sieve size) Leighton Buzzard sand and 9 mm ($\frac{3}{8}$–$\frac{5}{16}$ in. sieve

size) rounded pebbles (from the Bridport area of Chesil Beach) respectively. The 2 mm sand was stuck one layer deep to removable channel bed plates whilst the 9 mm pebbles were simply placed directly and tamped flat on the fixed wooden base of the channel. These three boundary roughness conditions are illustrated in figure 1 (plate 1). Further details of the bed roughness geometry are given in the experimental results section (§4) below.

2.3. *The hydrogen bubble technique*

This method of flow visualization and quantitative velocity measurement has been described in detail by Schraub *et al.* (1964) and in the particular form developed for the present work by Kemp & Grass (1967) and by Grass (1967).

In the present tests a fine $25\,\mu$ diameter platinum wire passed vertically through the channel bed in the centre of the channel at the test section. The lower end of the wire was fixed in a vertical traverse micrometer clamp below the bed of the channel and the wire was tensioned by means of a small weight suspended from the upper end of the wire above the water surface. The section of wire passing through the 5 cm depth of water was speck insulated, leaving gaps of approximately 1 mm, by paint spraying through a comb mask. A square wave 50 c/s pulsed negative voltage (approximately 30 V) was fed to the wire from a generator. An anode plate stuck to the side of the channel adjacent to the wire completed the electrolytic circuit.

Minute hydrogen bubbles were generated on the wire by electrolysis. The combination of speck insulation and pulsed voltage produced blocks of bubbles which were swept from the wire to form spatially organized flow tracers under intense illumination. A Vinten 250 frame per second medium high-speed motion camera was used to photograph the bubble tracers. Typical frames from the resulting films, showing the blocks of bubble tracers leaving the wire, are included in figures 8(*a*)–(*c*). As can also be seen in figures 8(*a*)–(*c*), the camera field of view covered an area of the flow extending approximately 3 cm out from the boundary. This was designed to include as large a portion of the important boundary regions of the flow as possible which was compatible with the somewhat exacting requirements of adequate object magnification and photographic definition necessary for the subsequent film analysis.

2.4. *Film analysis*

Point velocity samples were obtained by measuring the distance that the corner of a particular bubble block travelled in a short time interval of approximately $\frac{1}{50}$ second or the duration of 5 film frames. Longitudinal u and vertical velocities v were obtained in this manner. The fact that the flow tracers were spatially organized allowed a vertical line of blocks (figures 8(*a*)–(*c*)) to be followed *en masse*. This produced an adequate sample of instantaneous point u, v velocities spread out across the visible region of the boundary layer (15 u, v pairs in the smooth boundary test and 20 pairs in both the transitional and rough boundary experiments). The latter point velocity information in turn defined corresponding pairs of u, v velocity profiles. Examples of these instantaneous velocity profiles, which formed the basic data for subsequent analysis, are shown in figures 8(*a*)–(*c*).

Sequential pairs of u, v velocity profiles were obtained at approximately $\frac{1}{50}$ sec intervals (5 film frames) throughout the duration of the films.

The above velocity measurement procedure was made feasible by use of a d-mac co-ordinate analyser. The machine punched the bubble corner co-ordinate data directly onto paper tape for subsequent computer processing. In spite of this semi-automated procedure the film analysis time was still extremely lengthy. As a result, the sample sizes were restricted to 600 instantaneous u, v velocity profiles in the case of the smooth boundary test (12 sec of flow time) and 900 profiles in the cases of the transitional and rough boundary experiments (18 sec of flow time).

Measurement uncertainties associated with the hydrogen bubble technique have been discussed in considerable detail by Schraub *et al.* (1964) and more recently by Kim, Kline & Reynolds (1968). A similar appraisal of the possible sources of error inherent in the present velocity measurements suggested typical uncertainties in the individual instantaneous u, v values of approximately 3 and 10% respectively.

3. Experimental procedure

The flow rate was first adjusted to give an overall mean velocity of approximately 15 cm per second with a 5 cm depth flow at the test section. A fine ruled grid was placed in the camera field of view and photographed to determine the projection scale, boundary location and horizontal mean flow direction at the film analysis stage.

The wire traverse clamp was then adjusted to suitably position the first bubble block relative to the boundary and the wire cleaned using a small camel-hair brush and by voltage polarity reversal. With experience it proved possible to judge by eye when the wire was producing good quality clean-edged bubble blocks. The remainder of the 100 ft length of film was then exposed. At 250 frames per second the films took approximately 20 sec to run through the camera and good quality bubble production could usually be sustained over this short time interval. Two 100 ft lengths of Kodak 4x negative 16 millimetre film were exposed in each of the three experiments.

The packing geometry of the roughness elements immediately surrounding the wire was changed for the second of the two films in the transitional and rough boundary experiments. This reduced the chances of any extreme distortion in the averaged flow characteristics close to the bed, arising from an individual local packing pattern.

4. Experimental results

4.1. *General flow specification*

The basic flow data relating to the three experiments are set out in tables 1 and 2. Flow depths were measured relative to velocity origins determined from logarithmic plots of the mean velocity profile data for the transitional and rough boundary experiments (see §4.2 below). Mean flow velocities were calculated from the

volumetric discharge divided by the cross-sectional area. The approximately constant values of overall flow Reynolds number appear in the last column of table 1.

The total mean shear stress at a particular boundary distance was calculated from the sum of viscous shear, determined from estimates of the local gradient of

Experiment	Flow depth D (cm)	Mean flow velocity U (cm/sec)	Bed shear velocity u_τ (cm/sec)	Kinematic viscosity ν cm²/sec × 100	Flow Reynolds number $U.D/\nu$
Smooth boundary	5·13	14·0	0·88	1·064	6740
Transitional boundary (2 mm sand)	5·01	14·5	1·05	1·082	6700
Rough boundary (9 mm pebble)	4·97	14·6	1·22	1·098	6620

TABLE 1. Mean flow parameters

Experiment	Mean height of roughness tops above bed plate k (cm)	Standard deviation in k σ_k (cm)	Roughness Reynolds number $u_\tau k/\nu$	Height of velocity origin above bed plate (cm)
Smooth boundary	$\to 0$	$\to 0$	$\to 0$	
Transitional boundary (2 mm sand)	0·213	0·049	20·7	0·127
Rough boundary (9 mm pebble)	0·762	0·081	84·7	0·623

TABLE 2. Bed roughness parameters

mean longitudinal velocity, and directly measured Reynolds stress. Each of these local shear stress values was then linearly extrapolated to yield a value of mean shear stress at the boundary. The latter values, one for every boundary measurement point, were averaged to give a final measure of the mean bed shear stress relevant to each experiment. Boundary shear velocity values quoted in table 1 were derived from the latter mean bed shear stress results.

The average height k of the tops of the roughness elements above the base plate and the standard deviation σ_k in k are given in table 2. These data were obtained from a large sample of individual depth micrometer measurements. The roughness Reynolds numbers based on roughness height k appear in table 2. It can be seen that values quoted fall into the approximate transitional ($3 < u_\tau k/\nu < 70$) and rough ($u_\tau k/\nu > 70$) boundary categories based on Nikuradse's pipe data.

4.2. *Mean velocity profiles*

A primary concern when using the hydrogen bubble technique for quantitative measurement is the magnitude and extent of any bubble velocity defect caused by the wake downstream of the wire. Schraub *et al.* (1964) reported experiments which indicated negligible wake effect beyond 70 wire diameters. However, since the wake defect is likely to depend on a number of widely varying parameters including the extent of wire insulation, mark–space ratio of the voltage pulse generating the bubbles and Reynolds number, a direct calibration was carried out under the conditions of the present experiments.

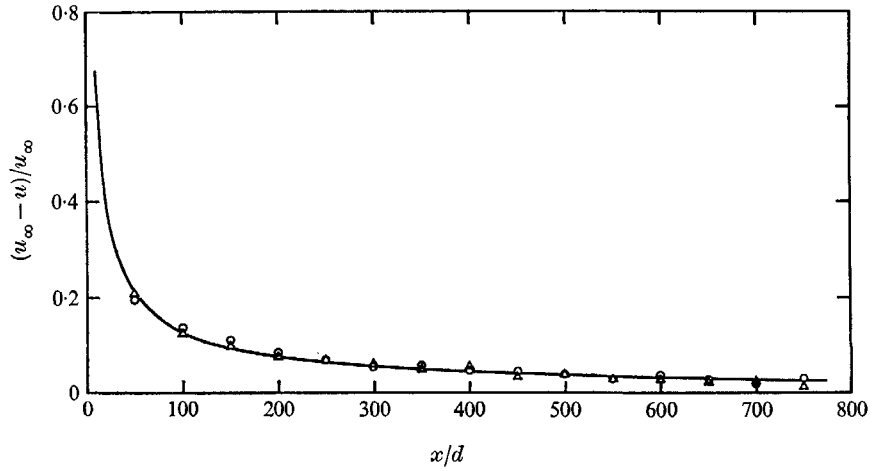

FIGURE 2. Empirical wake correction curve for the velocity defect downstream of the probe wire. Curve equation: $(u_\infty - u)/u_\infty = 3{\cdot}62\ (x/d)^{-0{\cdot}729}$.

The resulting plot of velocity defect versus wire diameter is shown in figure 2 in which u represents the bubble velocity at distance x downstream of the wire, diameter d, and u_∞ the undisturbed velocity derived from the limiting values of average bubble velocity measured at extreme downstream distances. Each of the two sets of data points plotted in figure 2 depicts the average of 40 individual bubble trajectories. It is interesting to note that while this curve shows velocity defects in excess of those reported by Schraub *et al.*, the defects are less than the centre-line values predicted for flow round an infinite cylinder at correspondingly low Reynolds number also reported by Schraub *et al.* The diminished velocity defect may be attributed both to a reduction in drag force caused by the bubble sheath round the wire and also to finite bubble diameter which tends to integrate the velocities across the wake width.

In the present study the majority of point velocity measurements were made between 100 and 300 wire diameters downstream, corresponding to a 13 to 6 % defect zone in figure 2. This velocity defect was considered sufficiently large to warrant compensation. A curve was therefore fitted to the defect data as shown in figure 2 and used to derive somewhat crude but satisfactorily accurate correction factors for the instantaneous longitudinal velocity measurements. This correc-

tion procedure was written into the computer programme which processed the raw co-ordinate data.

Average longitudinal velocity profiles derived from the overall samples of

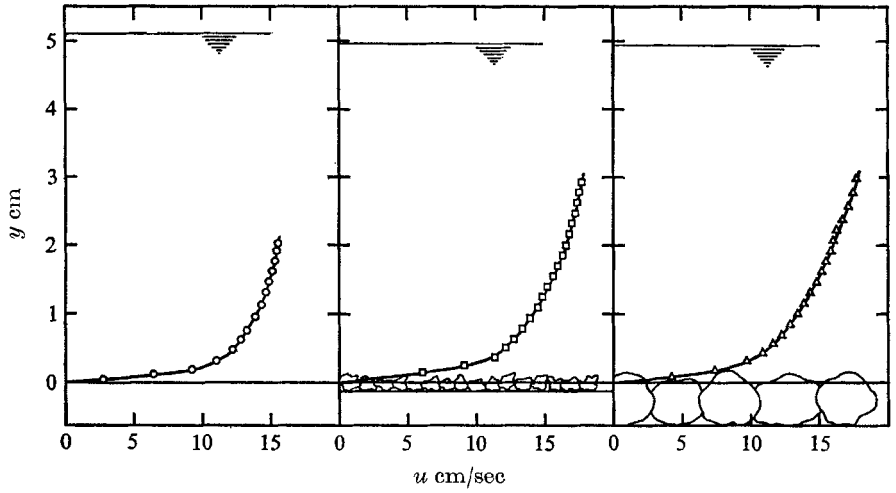

FIGURE 3. Mean velocity profiles. ○, smooth boundary; □, transitional boundary (2 mm sand); △, rough boundary (9 mm pebbles).

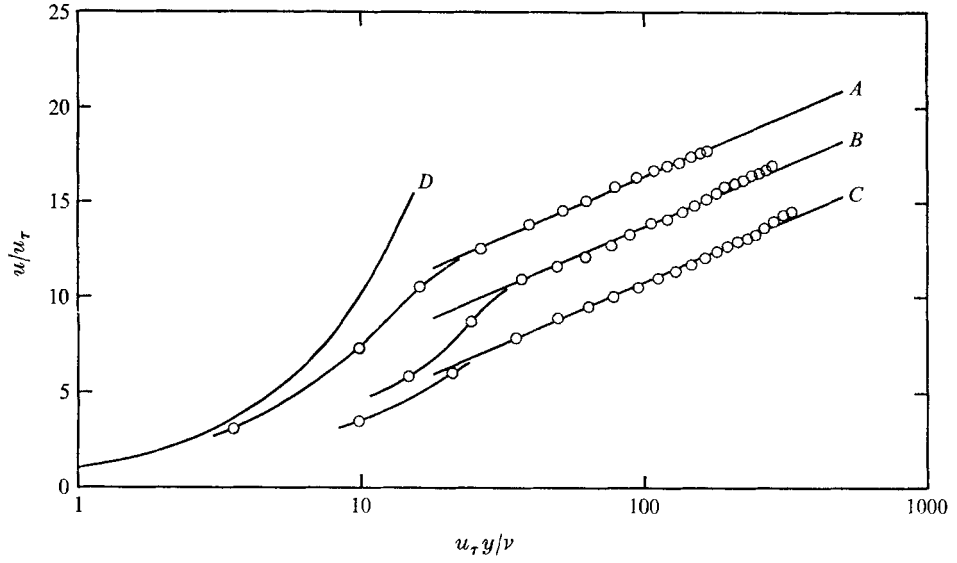

FIGURE 4. u/u_τ versus log $(u_\tau y/\nu)$. *A*, smooth boundary; *B*, transitional boundary (2 mm sand); *C*, rough boundary (9 mm pebbles); *D*, $u/u_\tau = u_\tau y/\nu$.

corrected instantaneous profiles are shown in figure 3. The velocity origins used in the case of the transitional and rough boundary conditions were obtained by shifting the ordinate (y) origin to yield the best straight line on a series of semi-logarithmic plots of the mean velocity data. As discussed by Clauser (1956), the

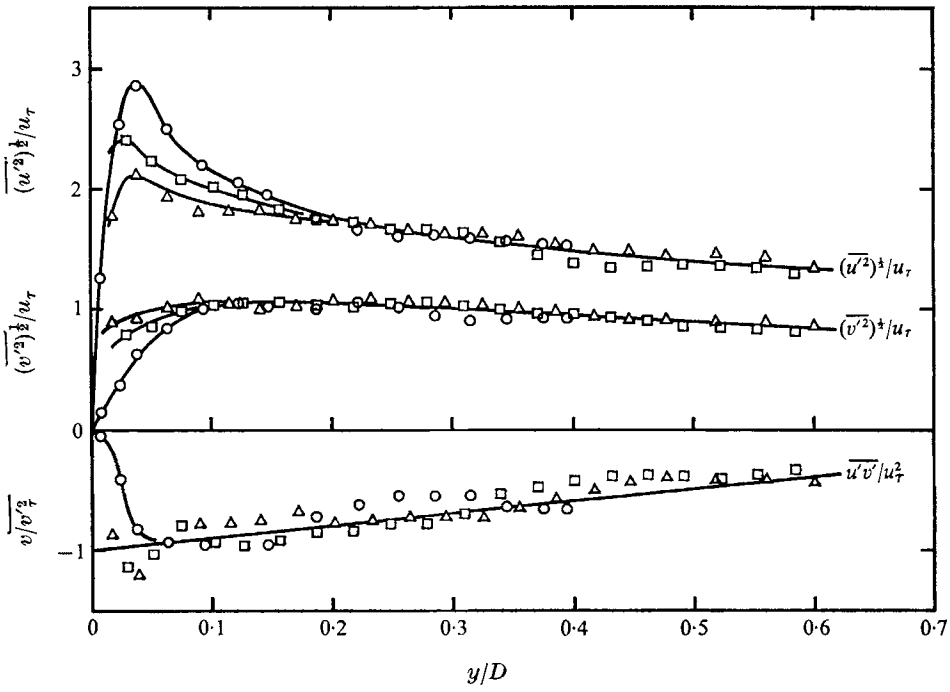

FIGURE 5. Turbulence intensity and Reynolds Stress. Same symbols as figure 3.

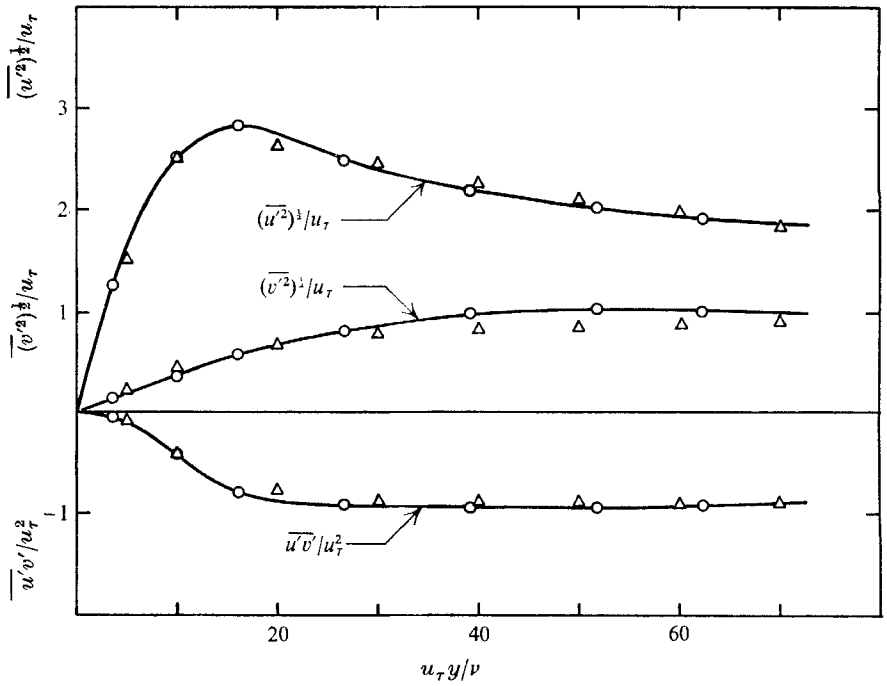

FIGURE 6. Wall region turbulence intensity and Reynolds Stress compared with Laufer's data for air flow in a pipe. ○, present smooth boundary data $Re = 6740$; △, Laufer's data $Re = 50\,000$.

latter method has the advantage of consistency and of producing y origins placed in a physically realistic position between the top and bottom of the roughness elements.

A semi-logarithmic plot of the longitudinal mean velocity data using wall region parameters appears in figure 4.

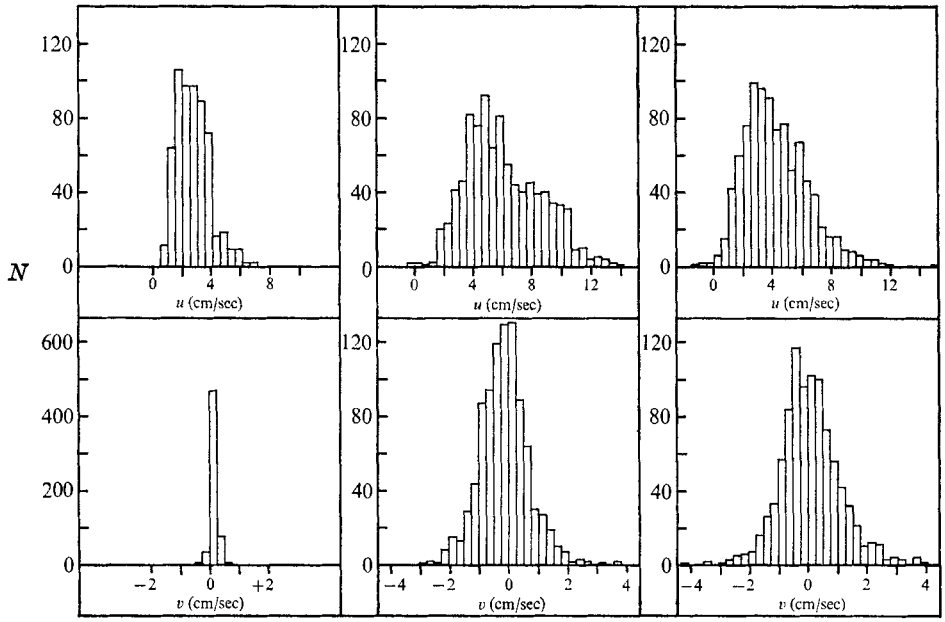

Smooth boundary	2 mm sand boundary	9 mm pebble boundary
y = 0·043 cm	y = 0·152 cm	y = 0·089 cm
$u_\tau y/\nu$ = 3·56	$u_\tau y/\nu$ = 14·79	$u_\tau y/\nu$ = 9·90
$\bar{u}$ = 2·75 cm/sec	$\bar{u}$ = 6·06 cm/sec	$\bar{u}$ = 4·25 cm/sec
$\bar{v}$ = +0·15 cm/sec	$\bar{v}$ = −0·15 cm/sec	$\bar{v}$ = +0·08 cm/sec
$(u'^2)^{\frac{1}{2}}$ = 1·11 cm/sec	$(u'^2)^{\frac{1}{2}}$ = 2·53 cm/sec	$(u'^2)^{\frac{1}{2}}$ = 2·16 cm/sec
$(v'^2)^{\frac{1}{2}}$ = 0·13 cm/sec	$(v'^2)^{\frac{1}{2}}$ = 0·83 cm/sec	$(v'^2)^{\frac{1}{2}}$ = 1·07 cm/sec
$(u'^2)^{\frac{1}{2}}/\bar{u}$ = 0·40	$(u'^2)^{\frac{1}{2}}/\bar{u}$ = 0·42	$(u'^2)^{\frac{1}{2}}/\bar{u}$ = 0·51
$S(u)$ = +0·75	$S(u)$ = +0·45	$S(u)$ = +0·76
$F(u)$ = 3·59	$F(u)$ = 2·65	$F(u)$ = 3·88
$S(v)$ = −0·13	$S(v)$ = +0·36	$S(v)$ = +0·28
$F(v)$ = 7·91	$F(v)$ = 4·49	$F(v)$ = 5·66
Total sample size = 592	Total sample size = 928	Total sample size = 933

FIGURE 7. Distributions of u, v velocity fluctuations close to the boundary. $S(u)$ = skewness factor = $\overline{u'^3}/(\overline{u'^2})^{\frac{3}{2}}$, $F(u)$ = flatness factor = $\overline{u'^4}/(\overline{u'^2})^2$, N = number of velocity measurements falling into the velocity intervals shown.

4.3. *Turbulence intensities and Reynolds stresses*

The longitudinal and vertical components of turbulence intensity and Reynolds stress, scaled with respect to boundary shear velocity, are shown plotted against boundary distance scaled by flow depth in figure 5. For comparison, the wall

region smooth boundary data are also plotted in relation to Laufer's (1952) pipe flow data ($Re = 50\,000$) using wall parameters in figure 6.

4.4. *Distributions of bed region velocity fluctuation*

Typical histogram plots of the longitudinal and vertical velocity fluctuations close to the boundary are shown in figure 7. The vertical ordinate represents the number of times out of the total sample that velocities were observed to fall in the intervals shown. Skewness and flatness factors and other data associated with these distributions are quoted in figure 7.

4.5. *Conditionally averaged velocity and Reynolds stress profiles*

As described in §2.4 above, the raw co-ordinate data derived from the film analysis were processed to yield sequential corresponding pairs of instantaneous longitudinal and vertical (u, v) velocity profiles examples of which are shown in figures 8(*a*)–(*c*).

Index	Smooth boundary			Transitional boundary			Rough boundary		
i	Y_i (cm)	Y_i/D	$Y_i u_\tau/\nu$	Y_i (cm)	Y_i/D	$Y_i u_\tau/\nu$	Y_i (cm)	Y_i/D	$Y_i u_\tau/\nu$
1	0·04(3)	0·008(4)	3·6	0·15(2)	0·030(4)	14·8	0·08(9)	0·017(9)	9·9
2	0·12	0·023	9·9	0·25	0·051	24·7	0·19	0·038	21·2
3	0·20	0·038	16·1	0·38	0·076	37·0	0·32	0·064	35·3
4	0·32	0·063	26·6	0·51	0·102	49·3	0·44	0·090	49·5
5	0·48	0·093	39·2	0·63	0·127	61·6	0·57	0·115	63·6
6	0·63	0·122	51·8	0·79	0·157	76·4	0·70	0·141	77·8
7	0·75	0·147	62·3	0·94	0·188	88·7	0·85	0·171	94·8
8	0·96	0·187	79·1	1·09	0·218	106	1·00	0·202	112
9	1·14	0·221	93·8	1·24	0·249	121	1·16	0·233	129
10	1·31	0·256	108	1·40	0·279	136	1·31	0·264	146
11	1·47	0·286	121	1·55	0·310	150	1·46	0·294	163
12	1·62	0·315	134	1·70	0·340	165	1·61	0·325	180
13	1·77	0·345	146	1·85	0·371	180	1·77	0·355	197
14	1·92	0·375	159	1·98	0·401	192	1·92	0·386	214
15	2·02	0·395	167	2·16	0·432	209	2·07	0·417	231
16	—	—	—	2·31	0·462	224	2·22	0·447	247
17	—	—	—	2·46	0·492	239	2·37	0·478	264
18	—	—	—	2·62	0·523	254	2·58	0·519	287
19	—	—	—	2·77	0·553	269	2·78	0·560	310
20	—	—	—	2·92	0·584	283	2·98	0·601	332

TABLE 3. Longitudinal velocity sampling locations used in the conditional averaging procedure

Each instantaneous u and v velocity profile was stored in the computer in the form of an array of u, v values interpolated at the fixed boundary distances Y_i given in table 3. The conditional sampling procedure adopted in the present tests selected u, v velocity profile pairs of the following two types: (i) those corresponding to maximum longitudinal velocity at a particular Y_i value, (ii) those corresponding to minimum longitudinal velocity at the same Y_i value.

One profile pair of each type was selected from a batch of 50 profile pairs (about 1 sec of the flow time). Thus in the case of the smooth boundary test, with a total sample size of 600 u, v profile pairs, 12 pairs of each type were selected at each Y_i

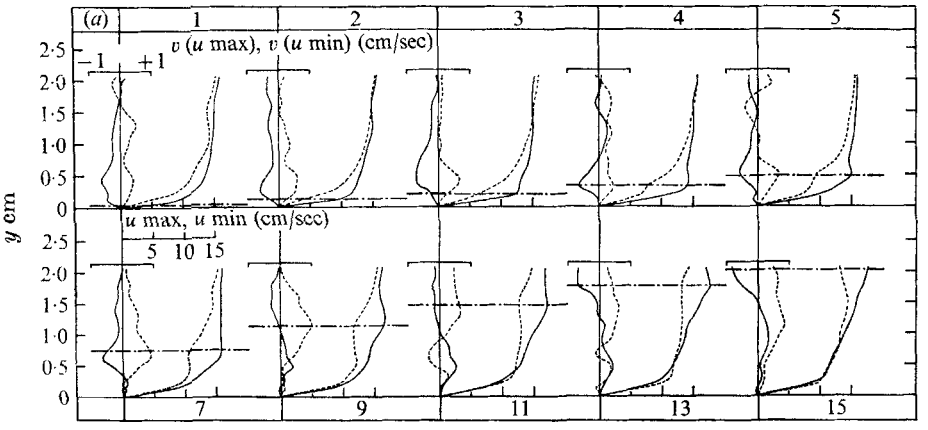

FIGURE 9(*a*). Smooth boundary experiment. Conditionally averaged instantaneous u, v velocity profiles u max, $v(u$ max); u min, $v(u$ min) at instants when the longitudinal velocity u is maximum and minimum respectively at the boundary distances Y_i marked by the horizontal dash-dot lines in the figure and given in table 3. The caption numbers are values of index i in Y_i and thus correspond with those in figure 10 for the same experiment. ———, u max, $v(u$ max); – – – –, u min, $v(u$ min).

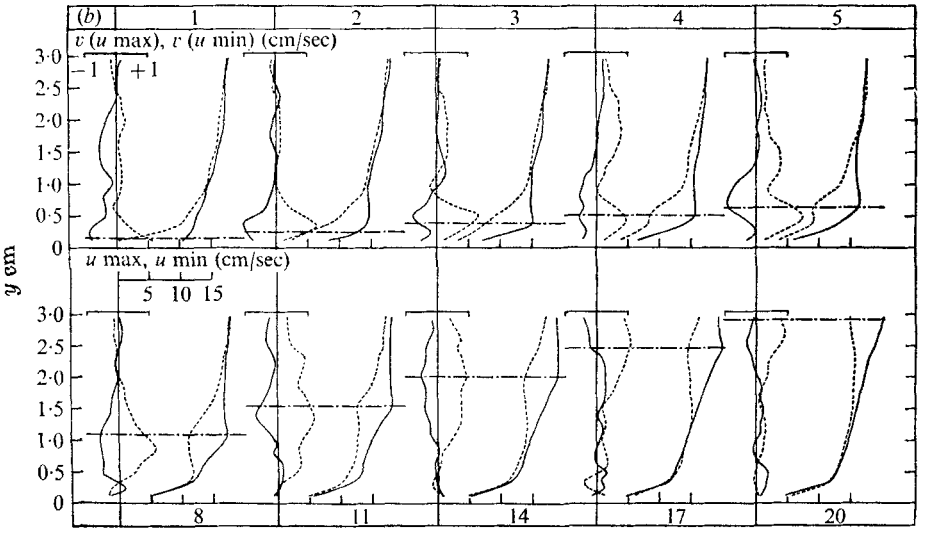

FIGURE 9(*b*). Transitional boundary experiment (2 mm sand), see caption to figure 9(*a*).

location. For the transitional and rough boundary tests conditional samples comprised of 18 profile pairs were selected from total samples of 900 pairs.

Ensemble averages of the conditional samples of instantaneous u and v velocity profiles corresponding to maximum and minimum u velocities occurring

at the various Y_i locations are denoted by u max, $v(u$ max) and u min, $v(u$ min) respectively, and are shown plotted in figures 9(*a*)–(*c*). Similarly, ensemble averages of instantaneous Reynolds stress contribution profiles computed from the conditional u, v profile samples, also associated with the occurrence of maximum and minimum longitudinal velocities at the various Y_i locations, are denoted by $u'v'/u_\tau^2$ (u max) and $u'v'/u_\tau^2$ (u min) respectively, and are plotted in figures 10(*a*)–(*c*).

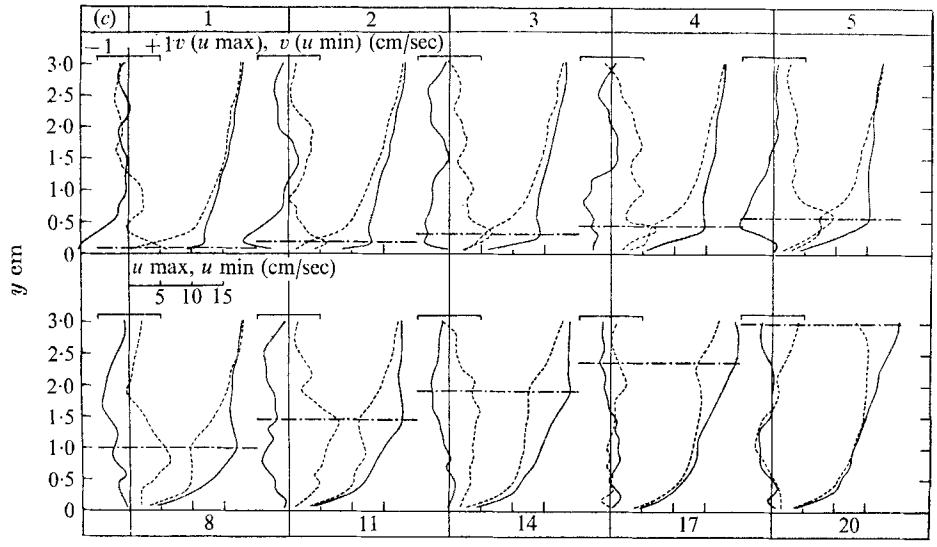

FIGURE 9(*c*). Rough boundary experiment (9 mm pebble), see caption to figure 9(*a*).

Individual data points have been omitted from figures 9 and 10 for the sake of clarity. The curves shown were, however, drawn through every data point without smoothing. Corresponding caption numbers (index i values) in figures 9 and 10 refer to corresponding Y_i locations and hence curves derived from the same conditional samples in each of the three experiments. Reynolds stress contributions in excess of a linear mean shear stress distribution have been shaded in figure 10 for emphasis.

5. Discussion

The concept of a boundary-layer eddy structure comprised essentially of coherent jets of fluid issuing from the boundary region and a more diffuse return flow is a common feature of models proposed by Townsend (1957, 1970), Grant (1958) and Lilley (1963). These models were derived from, and are therefore consistent with, many of the characteristics of the double velocity correlation function as measured, for example, by Favre *et al.* (1957, 1958), Grant (1958) and more recently by Tritton (1967).

As previously mentioned, the visualization studies reported by Kline *et al.* (1967), Kim *et al.* (1968) and by Corino & Brodkey (1969) draw attention to fluid

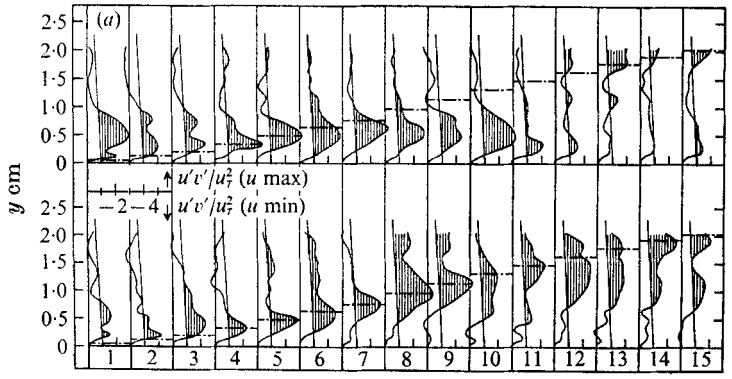

FIGURE 10(*a*). Smooth boundary experiment. Conditionally averaged distributions of Reynolds stress $u'v'/u_\tau^2$ (u max); $u'v'/u_\tau^2$ (u min) at instants when the longitudinal velocity u is maximum and minimum respectively at the boundary distances Y_i marked by the horizontal dash-dot lines in the figure and given in table 3. The caption numbers are values of index i in Y_i and thus correspond with those in figure 9 for the same experiment. The shaded areas represent Reynolds stress contribution in excess of a linear mean shear stress distribution.

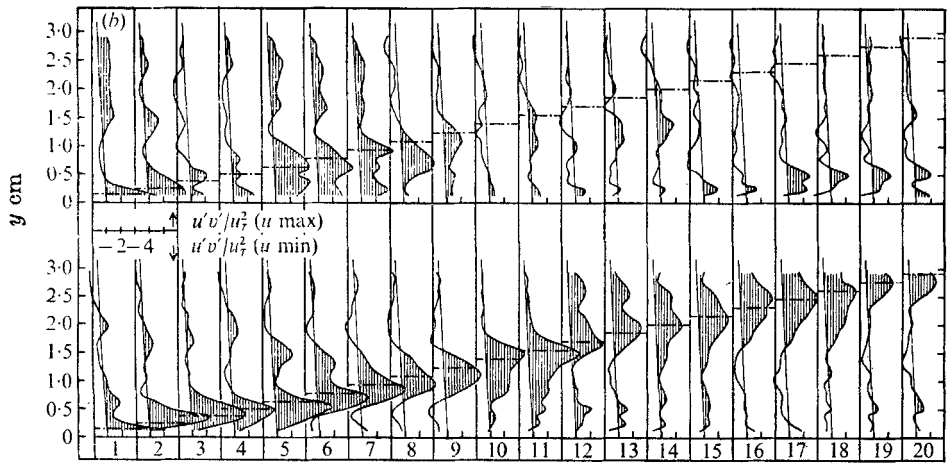

FIGURE 10(*b*). Transitional boundary experiment (2 mm sand), see caption to figure 10(*a*).

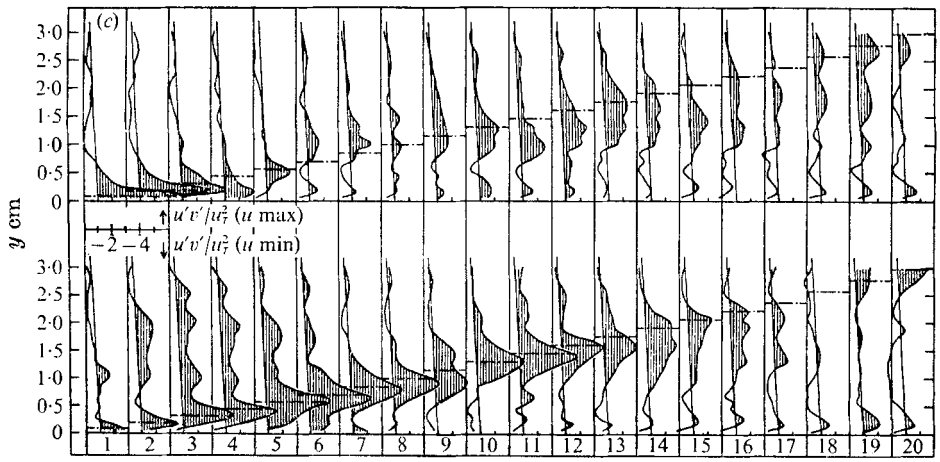

FIGURE 10(*c*). Rough boundary experiment (9 mm pebbles), see caption to figure 10(*a*).

ejection events which show some similarity to this simple jet model. In addition, however, the visual observations also strongly emphasize the randomly intermittent and cyclic nature of the overall process of turbulence energy production which includes the ejection sequences, and appears to be coupled with a repeating pattern of three-dimensional instability in the wall region.

Kovasznay *et al.* (1970) have speculated on the possible relevance of the viscous sublayer ejection phenomenon, observed by Kline *et al.*, to the process of entrainment in the intermittent region of the boundary layer. Other authors have also drawn attention to a possibly stronger structural connection between inner and outer boundary-layer zones than traditionally assumed. For example, Tritton (1967) has argued that the general similarity between observed features of correlation measurements in the inner and outer layers are more marked than the differences. Morrison & Kronauer (1969) have interpreted their wave transformation data, obtained from pipe flow experiments, as implying the presence of dominant energy containing eddies influencing the entire flow field, rather than being restricted to well-defined local regions. The suggested possibility, that a particular mode of momentum transport dominates a major portion of the total boundary-layer thickness and is basically represented by jets of low momentum fluid ejected from the boundary region and randomly distributed with respect to position and time, and the further possibility, that the general ejection process is a common feature of the flow structure irrespective of boundary roughness condition, form a background to discussion of the present results.

Since the Reynolds number was kept constant by maintaining constant depth and overall mean velocity in the channel throughout the three experiments differences in the measured flow properties are directly attributable to the differing boundary roughness conditions. Placing 2 mm sand and 9 mm pebbles on the boundary had the effect of increasing bed shear stress by approximately 40 and 90% respectively, relative to the smooth boundary shear stress (table 1).

As can be seen from figure 4, the mean velocity data conforms satisfactorily to straight line logarithmic representation. The empirically well-established logarithmic distribution confirms dimensional arguments which suggest that velocity gradient outside the viscous wall region is inversely proportional to boundary distance and directly proportional to boundary shear velocity. An increase in velocity gradient with increasing roughness and shear stress is an apparent feature of the mean velocity profiles shown in figure 3.

The smooth boundary turbulence intensity data (figure 6) is in good agreement with that produced by Laufer for the wall region of pipe flow ($Re = 50000$). No particular significance can be attached to this however in view of the considerable differences in intensity data reported by previous authors, including Clark (1968) and Morrison & Kronauer (1969), resulting from an apparent lack of universal scaling of turbulence data between pipe, channel and boundary-layer flow.

The turbulence intensity data are seen to scale directly with boundary shear velocity independent of the boundary roughness condition for $y/D > 0{\cdot}2$ (figure 5). This implies that, beyond a certain boundary distance, the turbulence intensity becomes dependent solely on boundary distance and boundary shear stress

but independent of the conditions producing the shear stress. However, immediately adjacent to the bed the data separate. With increasing boundary roughness the longitudinal intensity decreases whilst the vertical intensity increases.

The average Reynolds stress measurements, also shown in figure 5, exhibit rather more scatter than the intensity data. In spite of this the points show reasonably satisfactory correlation with a linear mean shear stress distribution attenuating to zero at the free surface as shown in figure 5. It would appear that the Reynolds stress measurements are more sensitive to the limited sample times used in the present tests than the other mean value quantities.

The histogram distributions shown in figure 7 demonstrate the wide range of longitudinal velocity fluctuations close to the boundary. Fluctuations between two and three times the local mean velocity occurred for all three surface roughness conditions. A feature common to each of the three longitudinal velocity distributions is the strong positive skewness in the bed region (figure 7). An additional influence of close bed proximity can be seen in the large flatness factors associated with the distributions of vertical velocity fluctuation also shown in figure 7. These large flatness factors reflect a tendency for the vertical velocity fluctuations to be more closely concentrated about the mean in the immediate bed region with infrequent but relatively very large positive and negative excursions.

Turning now to the conditionally averaged data, the linked pairs of conditionally averaged velocity profiles shown in figures 9(*a*)–(*c*) provide immediate quantitative confirmation of the visual impression of high longitudinal velocity inrush and low longitudinal velocity ejection phases referred to in §1 above. Minimum local longitudinal velocities are seen to be directly correlated with peaked regions of positive vertical velocity, a feature which is particularly noticeable close to the boundary. The regions of positive velocity spread out at the more extreme boundary distances. These observations are consistent with the ejection out from the boundary of 'lumps' of low momentum fluid to distances remote from the boundary. Similarly, maximum local longitudinal velocities correlate directly with peaked regions of negative vertical velocity. In this case, however, the effect tends to be concentrated closer to the boundary particularly for the transitional and rough boundary conditions. The latter observations confirm the visual impression of phases of fluid inrush towards the boundary.

These selectively averaged velocity profile measurements suggest very high positive contributions to local Reynolds stress values at all points out from the boundary through which the ejected lumps of fluid travel. Similarly, the inrush phases will also make a positive contribution to Reynolds stress but this effect is probably more restricted to the immediate boundary region. The latter implications are well confirmed by the Reynolds stress contribution profiles which reach peak values in excess of 5 times the local mean shear stress as shown in figures 10(*a*)–(*c*). When viewed *en masse* the Reynolds stress profiles associated with local minimum streamwise velocities or with the ejection phases, shown in the lower halves of figures 10(*a*)–(*c*), give a particularly strong visual impression of the migration of momentum deficient fluid, with its accompanying restraining influence, outwards from the boundary into the body of the flow.

By estimating the proportion of total time the flow in the region of smooth boundaries was disturbed by the observed ejection sequences, Corino & Brodkey (1969) were able to estimate that between 50 and 70% of the total local Reynolds stress could be accounted for by the resulting momentum transfer. Kim *et al.* (1968) made similar measurements and also concluded that a major proportion of Reynolds stress results from the sublayer ejection process. Corino & Brodkey further drew attention to the possibility that insweep phases of fast moving fluid towards the boundary might account for the differences between the actual Reynolds stress values and those estimated purely from the ejection sequences. The present smooth boundary data associated with high longitudinal velocities in the wall region and fluid inrush phases, shown in the upper portion of figure 10(*a*), clearly indicate a Reynolds stress contribution and hence turbulence production of the same magnitude as that produced during the ejection sequence in a region defined by $u_\tau y/\nu < 60$. This pattern is also repeated for the transitional and rough boundary conditions (figures 10(*b*), (*c*)).

The visual and quantitative evidence obtained in the present study strongly suggests that the fluid inrush phases could form a more important part of the general momentum transfer mechanism than has perhaps been previously recognized. The violence of the inrush phases is illustrated in figure 11 (plate 5). This shows a sequence of three frames from a 12-frame per second motion film recording the behaviour of flow in the viscous sublayer over a smooth boundary. The surface flow is visualized by intensively illuminated fine sand, diameter 0·1 mm, moving over the boundary. Arrow markers coincide with the position of a typical inrush phase which develops throughout the sequence, violently splaying the sand tracers forwards and to either side as it progresses along the bed. These photographs again show the streaky nature of the viscous sublayer flow so well illustrated by the visualization studies of Kline *et al.* (1967). Areas covered by dots in the photographs correspond to streaks of low-speed ejection fluid where the sand particles were moving very slowly. The elongated tracer lines are produced by fast moving sand particles along high velocity inrush streaks. This typical inrush sequence also clearly demonstrates the great longitudinal scale and short lateral scale of the eddies influencing the sublayer region. The latter observations are consistent with corresponding dimensions inferred from double velocity correlation measurements (Grant 1958, Tritton 1967).

The possible optimism expressed in continued attempts to interpret the apparent complexities of turbulent boundary-layer flow structure in terms of simple models has been largely sustained in the past by the high degree of structural order implied by velocity correlation measurements (Tritton 1967). Whilst the evidence presented in recent visualization studies reported by Kline *et al.*, Kim *et al.*, Corino & Brodkey and in the present paper tend to re-emphasize the considerable detailed structural complexity of the flow, the observations also suggest that certain basic features of the underlying structural mechanism can be described in relatively simple qualitative terms. Such a description exhibiting consistency with many of the structural features observed in both the present and previous studies cited above is given below.

Referring once again to the photographs presented in figure 11, it can be seen

that large lateral cross-flow velocities are produced along the sides of the high velocity streaks as the fluid is turned and spreads out over the surface. This stagnation-type flow pattern is inevitably accompanied by vortex stretching as suggested by Lighthill (1963). The longitudinal extent of these high velocity streaks ensures that there is a strong probability that they will occur immediately laterally adjacent to similar inrush streaks in spite of their overall random temporal and spatial distributions. The lateral flow of fluid along the adjacent sides of these high velocity streaks runs together. Low momentum fluid swept up and trapped between the streaks and seen as lines of sand dots in figure 11 is inevitably lifted and ejected from the boundary. As it travels outwards from the boundary, the low velocity fluid presents an obstruction to the higher velocity outer flow which has to pass over and round it. This produces inflexion points in the longitudinal velocity profiles clearly visible in both the instantaneous profiles of figures 8(*a*)–(*c*) and, more significantly in the conditionally averaged profiles of figures 9 (*a*)–(*c*).

Kim *et al.* (1968) drew attention to the similarities between these free shear layer velocity profiles and those occurring during laminar turbulent boundary-layer transition. In addition to primary instability the similarities appear to extend to the presence of secondary and tertiary instabilities taking the form of streamwise and spanwise vortices as observed by Kim *et al.* and also in the present study. Mollo-Christensen (1970) has further suggested that the discrepancy which exists between the disturbance growth rate predicted by linear theory as compared with observation could be due to a strong interaction between the many scales of motion present in such a hierachy of instabilities.

The zones of large longitudinal velocity defect and local vorticity maxima associated with the instantaneous inflexion-point velocity profiles must render them highly unstable, if only to the influence of the subsequent gradual acceleration produced by drag and pressure forces exerted by the higher velocity fluid to either side and following up behind the region. That some more violently catastrophic inward collapse of the boundary layer takes place is supported by the following three observations in addition to the evidence discussed above relating to figure 11.

First, as previously mentioned, the maximum longitudinal velocities occurring close to the boundary are strongly and locally correlated with large negative vertical velocities directing fluid inwards towards the boundary, as shown in the upper portions of figures 9(*a*)–(*c*). Negative peaks in the vertical velocity profiles are particularly prominent around $y = 0{\cdot}6$ cm for all three boundary roughness conditions.

Second, the large streamwise velocities occurring in the bed region are also associated with local points of extremely high curvature and abrupt changes of slope on the longitudinal velocity profiles as shown in figures 9(*a*, 2, 3, 4, 5); 9(*b*, 2, 3, 4, 5); 9(*c*, 2, 3, 4, 5, 6). This indicates rapid fluid acceleration with little time for either viscous or small eddy momentum transfer to erode the points of high curvature which might be expected close to the boundary during a more gradual acceleration phase.

Third, a feature common to data from all three boundary roughness

conditions is the strong positive skewness in the distributions of longitudinal velocity fluctuation close to the bed (figure 7). In addition, measured distributions of fluctuation in the time derivative of longitudinal velocity, obtained during a recent series of tests on bed sediment stability (Grass 1970), also revealed positive skewness factors as high as 1·5 at $u_\tau y/\nu$ values of approximately 4.

The above observations emphasize the great intensity of the inrush phases which can certainly not be described as a diffuse return flow close to the bed. Indeed, the overall picture lends support to the proposition that the inrush phases could form an essential part of the cycle by which energy is abstracted from the mean flow and fed into the turbulence structure; a cycle which includes the resulting ejection of fluid outwards from the boundary. Whether or not the fluid lifted and ejected from the inner boundary region traverses the entire boundary-layer thickness under its initial vertical momentum remains uncertain. Kim *et al.* have drawn attention to a violent oscillatory interaction between the ejected fluid and the faster flowing fluid it displaces. This interaction could well reflect some instability process whereby the vertical ejection velocities are amplified. It certainly appears possible that the high velocity fluid passing over the top of the low-speed ejection regions, indicated in the velocity inflexion profiles shown in figures 9 (*a*), (*b*), (*c*; 4), for example, could produce a local pressure distribution favourable to amplification of the initial ejection disturbances. In this connexion it is also interesting to note that for the smooth boundary test maximum streamwise velocities occurring at boundary distances greater than approximately $y = 0{\cdot}75$ cm ($u_\tau y/\nu = 62$) begin to be occasionally linked with low streamwise velocities and positive vertical ejection velocities close to the boundary, as seen in figures 9(*a*; 7, 9, 11). The large positive contribution to Reynolds stress around $y = 0{\cdot}5$ cm, shown in the upper portion of figure 10 (*a*; 10) ($Y_i = 1{\cdot}31$ cm), for example, includes a 40% ejection contribution as indicated by detailed analysis of the 12 individual instantaneous u, v velocity profile pairs making up the relevant conditional sample. These individual sets of data also revealed instances of large negative local contributions to Reynolds stress usually correlating with the movement of fluid with high streamwise velocity away from the boundary.

Differences in the inrush and ejection sequences between the smooth and rough boundary flows appeared to be mainly associated with the detailed mechanics of low momentum fluid entrainment at the bed surface, following inrush phases. In this respect it is envisaged that the smooth boundary viscous sublayer fluid and the fluid trapped between the roughness elements simply forms a 'passive' reservoir of low momentum fluid which is drawn on during ejection phases. Entrainment was extremely violent in the rough boundary case, with ejected fluid rising almost vertically from between the interstices of the roughness elements. The long twisting streamwise vortices, very apparent close to the smooth boundary during inrush ejection cycles, were also much less conspicuous in the transitional and rough boundary flows. It therefore appears possible that different dominant modes of instability might prevail for different boundary roughness conditions.

Certain observed features of the turbulence and mean flow characteristics

can be interpreted in the light of the intermittent inrush ejection-type structural model discussed above. For instance, during an inrush phase the fluid with high streamwise velocity very close to the bed is arrested mainly by viscous shear in the case of smooth boundary flow and hence will decelerate much more slowly than in the cases of transitional and rough boundary flow, where form drag creates a more effective arrest mechanism. It might be anticipated therefore that the bed region longitudinal component of turbulent intensity would decrease with increasing bed roughness which is confirmed by the data plotted in figure 5. Continuity requirements, on the other hand, must accentuate the vertical intensities in the case of increasing boundary roughness where the longitudinal arrest mechanism is increasingly effective over much shorter streamwise distances. This expectation is also confirmed by the present data. The improved efficiency of the fluid arrest mechanism with increasing bed roughness and resulting longitudinal localization of the inrush ejection cycle could also account for the corresponding increases in Reynolds stress contributions observed in figures 10(*a*)–(*c*).

Whilst the vertical velocities associated with the ejected lumps of fluid (figures 9(*a*)–(*c*)) show some attentuation as they traverse the visible section of the flow field, they remain sufficiently strong to imply continued influence of the ejection mechanism throughout the entire flow depth. This conclusion was supported by the observed presence of boils of fluid on the free surface which became more pronounced with increasing boundary roughness. The concept of ejected lumps of low momentum fluid with normal velocity component progressively attentuated by drag forces as their distance from the boundary increases is consistent with the decreasing rate of growth in thickness of free stream boundary layers with streamwise distance. The observed rapid response of the inner layer zones to sudden changes in boundary roughness, discussed by Clauser (1956) and Rotta (1961), similarly reflects the rapid redistribution of effective shear stress expected, with wall region ejection velocities as high as 10 % of the longitudinal velocity (figures 8(*a*)–(*c*) and 9(*a*)–(*c*)). Clauser and Rotta also drew attention to the relatively slow response of the outer flow layers to sudden local changes in conditions at the bed. According to the ejection mechanism, this can be interpreted as being due to the outer flow regions only reacting to ejections which leave the boundary considerable distances upstream and are therefore largely independent of local conditions.

Whilst the inrush phases are most strongly associated with a region close to the boundary, the accompanying negative vertical velocities exhibit very significant positive correlation over considerable y distances as shown in figure 9(*a*; 1, 2, 3), for example. This suggests a further connexion between inner and outer flow layers in addition to the ejection process. The interaction between the two layers, and in particular the response of the inner layer, could thus be affected by the overall flow boundary conditions influencing the outer regions. This is consistent with the observed lack of universal scaling of turbulence characteristics, by wall parameters, between pipe, channel and zero pressure gradient boundary-layer flows which led Townsend (1957) to introduce the concept of 'universal' and 'irrelevant' motion. Bradshaw (1967), in discussing

Townsend's concept, has demonstrated how a similar driving link between outer and inner flow regions need not significantly affect the distributions of mean shear stress and velocity, which are observed to scale universally, but would contribute for example to turbulence intensity.

In the case of smooth boundary flow Kline *et al.* (1967) have reported a lateral spacing of wall velocity streaks, associated with the inrush ejection eddies, of order 100 times the wall-region viscous length scale ν/u_τ. This is in agreement with the spacing indicated in figure 11. It is postulated that as boundary roughness scale, and hence displacement thickness and the extent of the zone of appreciable mean velocity defect in the boundary region, increase, the overall scale of the inrush and ejection eddies should also increase. Some visual evidence of such an effect was apparent from comparative inspection of the film records in the present experiments. Further confirmation is afforded by the large-scale structure of wind in the ground region atmospheric boundary layer. This is commonly visualized by the relatively large elongated patterns of ripple disturbance formed on near-shore water surfaces by off-shore winds and also by the streaky elongated swirling motion of sand blown along beaches or powdered snow blown over locally flat surfaces. The scale of these ground region eddies reflects the natural roughness scale of the surrounding terrain. For example, the volume of eddies involved in the inrush ejection cycle will be larger over city centres than over flat open countryside, corresponding to greatly increased roughness, boundary shear stress and displacement thickness.

To conclude, there are aspects of the structural model discussed above, particularly relating to the form of instability associated with the inrush and ejection sequences, which remain objects of speculation. However, certain other features, including the presence of an apparently universal ejection-type momentum transport mechanism possibly extending across the entire thickness of the boundary layer, appear to be strongly supported by the evidence presented in both the present paper and the previous studies cited.

The author is indebted to Dr P. H. Kemp for his help and advice during the course of this study. The work was supported by grants from the British Science Research Council.

REFERENCES

BRADSHAW, P. 1967 *J. Fluid Mech.* **30**, 241.

CLARK, J. A. 1968 *J. Basic. Engng. A.S.M.E.* paper 68-FE-26 p. 1.

CLAUSER, E. H. 1956 *Advances in Applied Mechanics*, vol. IV, p. 1. Academic.

CORINO, E. R. & BRODKEY, R. S. 1969 *J. Fluid Mech.* **37**, 1.

FAVRE, A., GAVIGLIO, J. & DUMAS, R. 1957 *J. Fluid Mech.* **2**, 313.

FAVRE, A., GAVIGLIO, J. & DUMAS, R. 1958 *J. Fluid Mech.* **3**, 344.

GRANT, H. L. 1958 *J. Fluid Mech.* **4**, 149.

GRASS, A. J. 1967 Ph.D. Thesis, London University.

GRASS, A. J. 1970 *J. Hyd. Div. A.S.C.E.* vol. 96, no. HY3, paper 7139 p. 619.

KEMP, P. H. & GRASS, A. J. 1967 *Proc. 12th Congress I.A.H.R.* vol. 2, p. 201.

KIM, H. T., KLINE, S. J., & REYNOLDS, W. C. 1968 Dept. of Mech. Eng. Stanford Univ. *Rep. MD*20.

KLINE, S. J., REYNOLDS, W. C., SCHRAUB, F. A. & RUNSTADLER, P. E. 1967 *J. Fluid Mech.* **30**, 741.

KOVASZNAY, L. S. G., KIBENS, V. & BLACKWELDER, R. F. 1970 *J. Fluid Mech.* **41**, 283.

LAUFER, J. 1952 *N.A.C.A. Rep.* no. 1174.

LIGHTHILL, M. J. 1963 *Laminar Boundary Layers*, (ed. L. Rosenhead) p. 98. Clarendon.

LILLEY, G. M. 1963 *Cranfield Inst. of Tech.* Note no. 140.

MOLLO-CHRISTENSEN, E. 1970 *A.I.A.A. 7th Annual Meeting*, Paper no. 70–1308.

MORRISON, W. R. B. & KRONAUER, R. E. 1969 *J. Fluid Mech.* **39**, 117.

ROTTA, J. C. 1961 *The Mechanics of Turbulence*, p. 255. Gordon and Breach.

SCHRAUB, F. A., KLINE, S. J., HENRY, V., RUNSTADLER, P. W. & LITTLE, A. 1964 Dept. of Mech. Engng. Stanford Univ. Rep. MD10. *Trans. A.S.M.E.*, Series D, **87**, 429.

TOWNSEND, A. A. 1957 *Symp. Int. Union of Theor. and Appl. Mech.* p. 1. Springer.

TOWNSEND, A. A. 1970 *J. Fluid Mech.* **41**, 13.

TRITTON, D. J. 1967 *J. Fluid Mech.* **28**, 439.

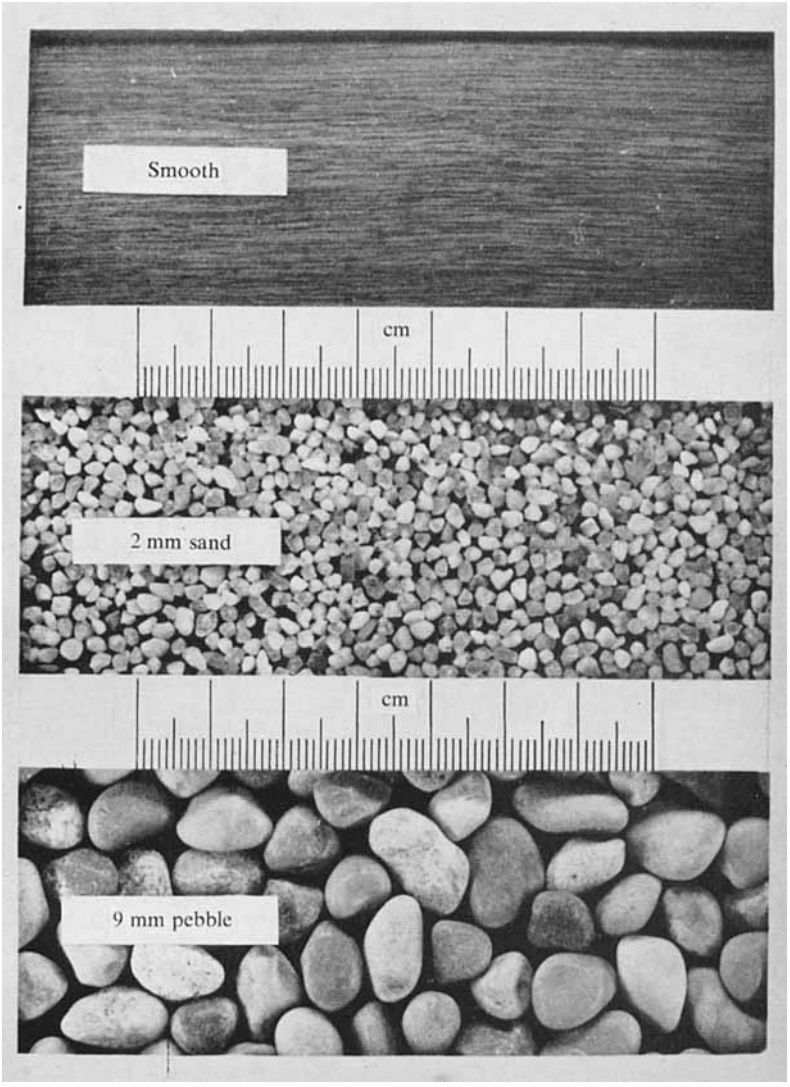

FIGURE 1. Boundary roughness conditions.

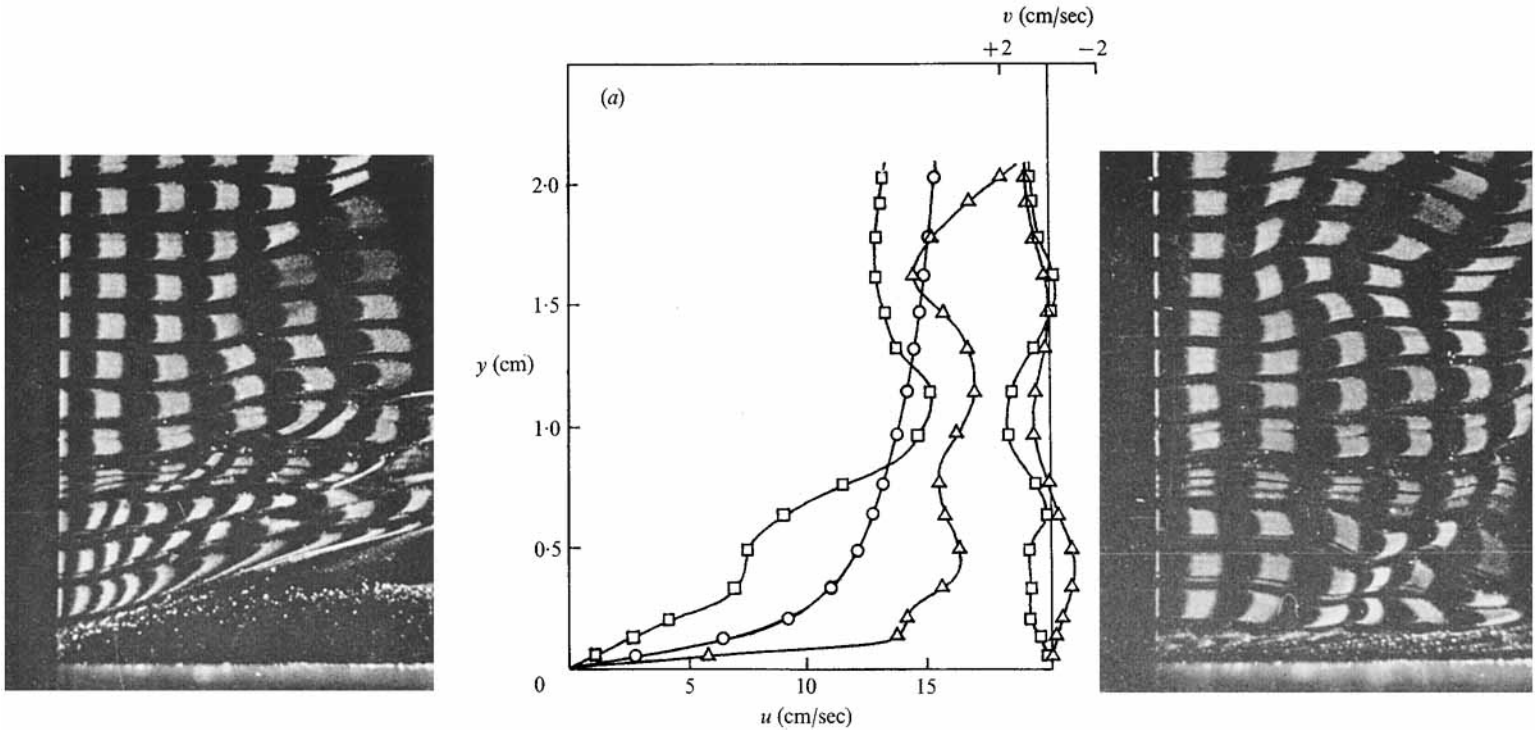

FIGURE 8(*a*). Smooth boundary experiment. Typical film frames with corresponding instantaneous u, v velocity profiles. □, u, v velocity profiles associated with low boundary velocity and a fluid ejection phase (photograph on left); △, u, v velocity and a fluid inrush phase (photograph on right); ○, mean longitudinal velocity profile for comparison.

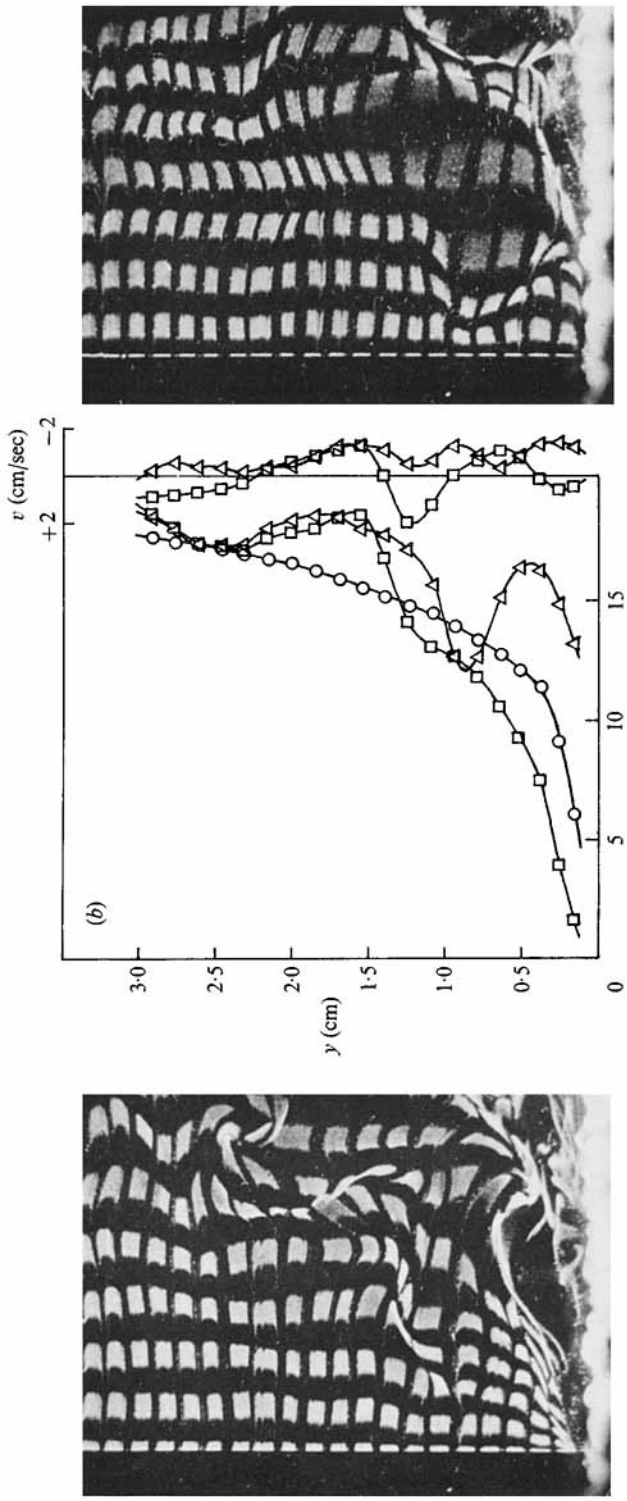

FIGURE 8 (*b*). Transitional boundary experiment (2 mm sand), see caption to figure 8 (*a*).

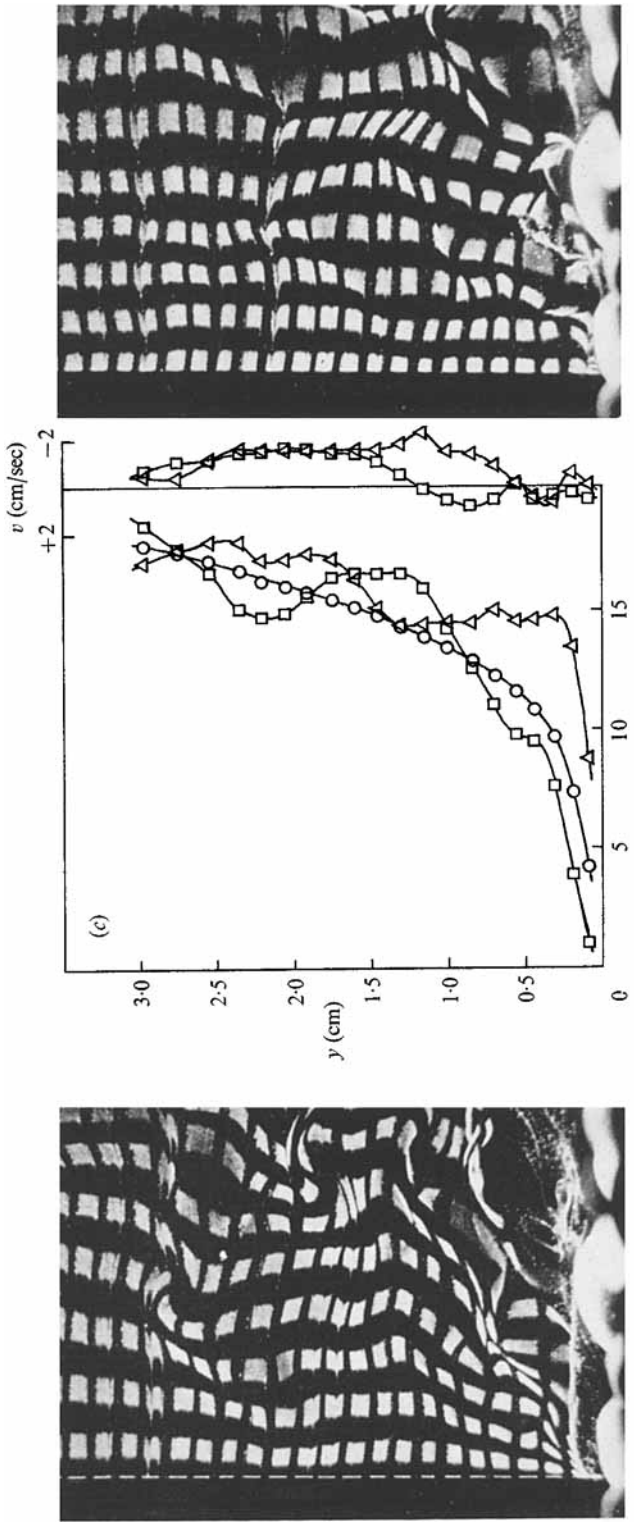

FIGURE 8 (*c*). Rough boundary experiment (9 mm pebbles), see caption to figure 8 (*a*).

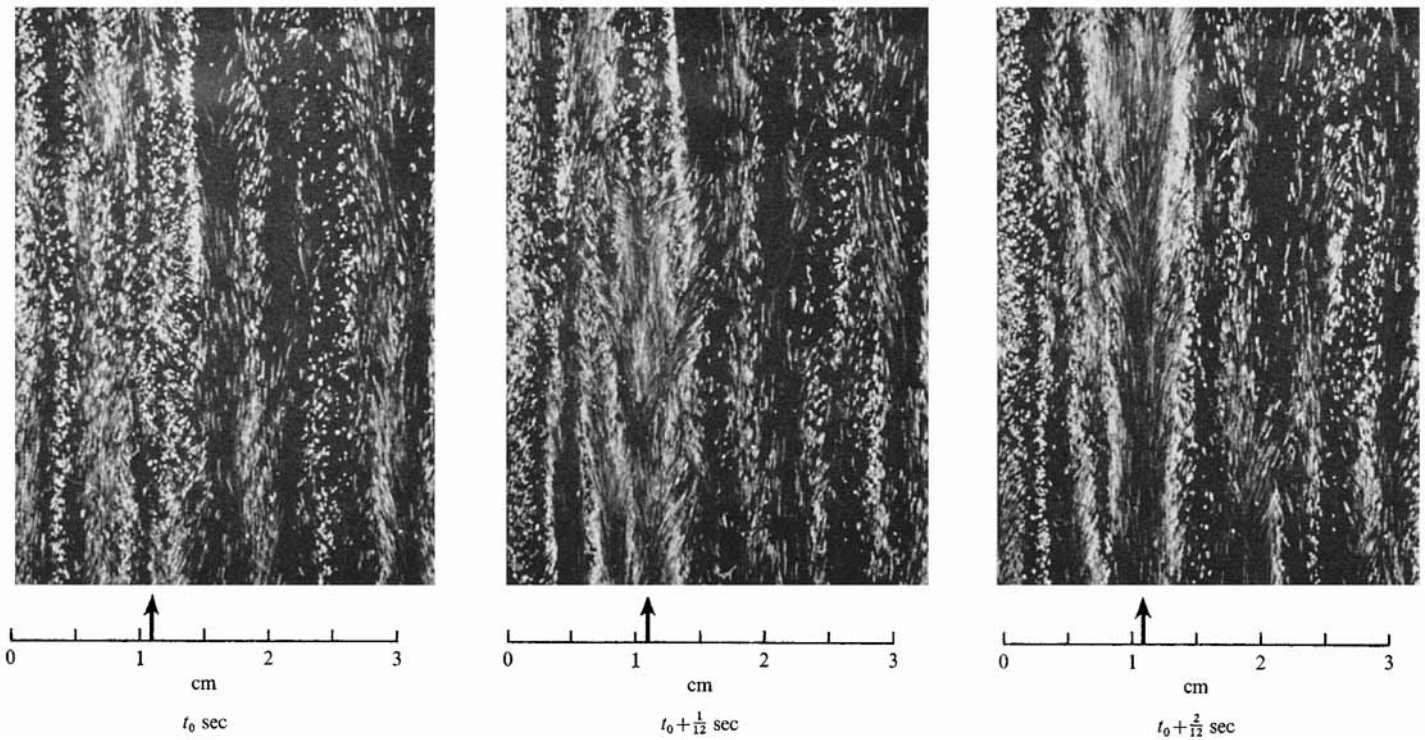

FIGURE 11. Viscous sublayer flow structure visualized by means of fine 0·1 mm diameter sand moving over a smooth black boundary. The sequence of three motion film frames, separated in time by $\frac{1}{12}$ sec. with a $\frac{1}{30}$ sec exposure, illustrate the development of a typical fluid inrush phase, indicated by the arrow. $\nu = 0{\cdot}0125$ cm^2/sec, $u_\tau = 2{\cdot}13$ cm/sec, $\nu/u_\tau = 0{\cdot}006$ cm.